

Effect of the Morphology of Electrospun Polyvinylidene Fluoride Nanofiber on Corrosion Property of Q345 Steel

Yuhua Dong^{*}, Siyi Li, Qiong Zhou

College of Science, China University of Petroleum (Beijing), Beijing 102249, China

*E-mail: dyhydt@yahoo.com

Received: 26 May 2017 / *Accepted:* 28 September 2017 / *Published:* 12 November 2017

Different contents of polyvinylidene fluoride (PVDF) nanofiber membranes were electrospun on Q345 steel surface. Nanofiber morphology was observed via scanning electron microscopy. The samples were immersed in 3.5 wt. % solutions, and an electrochemical workstation was used to investigate the anticorrosion performance of the nanofiber membranes. Electrochemical impedance spectroscopy measurements indicated that the electrospun PVDF nanofiber membranes effectively protected the Q345 steel. Nanofiber morphology significantly influenced its protection property. The nanofiber membranes with uniform thickness exhibited better performance than the membranes with a beaded structure. The nanofiber membrane included in the epoxy resin composite coating improved protection performance of the coating.

Keywords: Electrospun; Nanofiber membrane; EIS; Corrosion

1. INTRODUCTION

Electrospun is a well-known and versatile technique to produce micro- and nanofibers. In this process very fine and continuous fibers are formed from an electrically charged jet of polymer solutions or melts when the electrostatic forces overcome the surface tension of the polymeric fluid. The nanofibers have numerous excellent properties, such as good mechanical strength, high flexibility degree and large surface area-to-volume ratio; they have been extensively used in the medical, energy, engineering and nano-industry fields [1-5].

In recent years, the technology that utilizes the electrospun method to prepare nanofiber membranes has become a new method for corrosion protection. Results of several references indicated that electrospun polyvinyl alcohol, polyvinyl chloride and polystyrene membrane could protect aluminum, steel and brass against corrosion [5-7]. Electrospun polylactic acid (PLA) was also

demonstrated to improve the corrosion resistance of Mg-based implant materials [8]. Polyaniline (PANI)/poly (methyl methacrylate) (PMMA) microfibers film was electrospun on the surface of carbon steel. This electrospun film had enhanced anticorrosion performances in comparison with the drop-cast PANI/PMMA film because of its extraordinary compact microstructure [9]. Complicated electrospun technologies, such as blended electrospun or electrospun block copolymer, were also studied. Menchaca [10] had electrospun nylon 6-6 fiber with inhibitor benzotriazole to make it as an inhibitor nanocontainer. Polycaprolactone (PCL) /ZnO NPs were electrospun on AZ31 Mg alloy surface to enhance corrosion resistance and biocompatibility of the Mg alloy [11]. Grignard investigated the electrospun diblock copolymer of poly (heptadecafluorodecylacrylate-co-acrylic acid) random copolymer and polyacrylonitrile. The results indicated that the nanofiber exhibited excellent corrosion resistance [12]. In addition, studies had applied the coaxial electrospun technology to prepare core-shell structure fiber, and a healing agent was encapsulated in the core fiber to investigate its self-healing capability [13-17].

The aforementioned references examined the protection performance of nanofiber with one type of morphology. Electrospun fiber morphology can be influenced by the concentration of a solution (which plays a visible role), applied voltage, collection distance, flow rate and so on [18-21]. None of them investigated protection performance of different morphology for electrospun fiber. In this study, the effect of the morphology of electrospun nanofiber on its anticorrosion performance for metals was studied. Polyvinylidene fluoride (PVDF) was selected as the electrospun material because of its strong polarity, chemical corrosion resistance and excellent mechanical properties [22-23]. Different contents of PVDF nanofiber membranes were electrospun on Q345 steel surface. Some of the samples were spin-coated with epoxy resin on the surface of the nanofiber membrane to prepare the composite coating. An electrochemical workstation was used to investigate their anticorrosion performance.

2. EXPERIMENTAL

2.1. Sample preparation

Q345 steel (0.12%-0.20% C, 0.20%-0.60% Si, 1.20%-1.60% Mn, 0.030% S, $\leq 0.030\%$ P, in mass%) was used to prepare the work electrode. The working electrode was embedded in epoxy resin within a PVC tube. The electric contact was obtained by soldering a copper wire on the back of the working electrode. The working surface had an area of 1.13 cm^2 . The electrodes were ground using emery paper (1000 grit).

2.2 Nanofiber Membrane preparations

PVDF (Kynar Flex 2801, $M_n = 155,000$ and $M_w = 470,000$) was purchased from Arkema S.A. (France). Dimethyl formamide (DMF) and acetone were acquired from Beijing Chemical Works (China) and were used as received without further purification.

PVDF was dissolved in a mixed solvent of DMF/acetone (7:3, V/V) to obtain 12, 15, 17 and 20 wt. % solutions, which were magnetically stirred for 5-6 h at 60 °C. During electrospun, the solution was fed in a 10 mL syringe to which a capillary tip of 0.52 mm inner diameter was attached and a voltage of 12 kV was applied to draw the nanofibers from the prepared solutions. The distance between the needle tip and the collector was 15 cm. The electrospun fibers were accumulated on Al foil for 5 min to observe the morphologies by SEM, and accumulated on electrode surfaces for 20 min to test the corrosion resistance by EIS. The resultant PVDF fibrous membranes were then dried under vacuum at 80 °C for 5 h to remove the residual solvent before further use. The electrospun condition was at room temperature and with 20% humidity.

2.2 Epoxy coating preparation

PVDF was first electrospun directly onto a 1.13 cm² surface of the working electrode. To introduce the epoxy matrix, epoxy resin based on bisphenol-A with an epoxy value of 0.51 mol/ (100 g) was chosen (E-51 from Fenghuang Epoxy Resin Factory, Wuxi, China). Curing agent (NX-2003D) was added to the epoxy resin with a mass ratio of 3:10 (purchased from Cardolite Chemical Co. (Zhuhai, China)). The mixture was then spin-coated on PVDF-coated electrode or bare electrode using a spin processor. The spin program was set as follows: 500 rpm for 20 s, then 1000 rpm for 30 s. The coatings were finally cured at 80 °C for 8 h. The thickness of the coatings was about 100 µm.

2.4. Electrochemical impedance spectroscopy (EIS) measurement

The electrodes (the bare electrode, the electrodes deposited with different contents of PVDF electrospun nanofiber membrane, and the electrode deposited with PVDF electrospun nanofiber membrane and epoxy resin) were immersed in 3.5 wt. % NaCl neutral solutions at room temperature. There was always a parallel sample for the every electrode. EIS measurement was characterized using an electrochemical workstation (Reference 600, Gamry Instruments, US), over a frequency range of 10⁻²-10⁵ Hz at open circuit potential, and with a 10 mV AC perturbation. Inside a Faraday cage, a three-electrode system was established, consisting of the coated specimen as the working electrode, a carbon rod as the counter electrode and saturated calomel Hg-Hg₂Cl₂ electrode (SCE) as the reference electrode. The EIS was measured at different immersion days to assess the degradation of the barrier properties of the coatings.

2.5. Characterization

The morphologies of the nanofiber and the corroded metal surface were analyzed via scanning electron microscopy (SEM, Quanta 200F, and FEI Holland). Fiber diameter distribution was evaluated using Nano Measurer software.

3. RESULTS AND DISCUSSION

3.1. Morphology of the electrospun PVDF nanofiber

The concentration of solution has an important effect on the morphology of the nanofiber, because it controls viscosity and surface tension of the solution. The SEM images of different contents of PVDF nanofiber and the distribution of fiber diameter are shown in Fig. 1.

The electrospun PVDF membrane showed a fully interconnected porous structure composed of lots of ultrafine fibers. Fiber diameter evidently increased with PVDF content [24]. The presence of beads in electrospun fibers was found for 12% PVDF (Fig.1a). That was because of low content of PVDF and without enough entanglement between molecular chains. The viscosity and surface tension of the solution decreased. The droplets of the solution had got to the collector before the solvent evaporated completely. The beads disappeared with increasing of PVDF content. For the 15% PVDF nanofiber membrane, the content and viscosity increased, fiber thickness was uneven (Fig. 1b). However, nanofiber thickness became uniform and dense (Fig. 1c) for the 17% PVDF nanofiber membrane. It was due to increase of viscosity and surface tension of the solution, the stable jet could be formed and deposited on the collector in the form of fiber. When the content was 20%, the solution viscosity was so high that the electric field force couldn't make the droplets thoroughly split into thin thread. It caused a lamellar structure to be evident (Fig. 1d), and the nanofibers were mutually interconnected and porous.

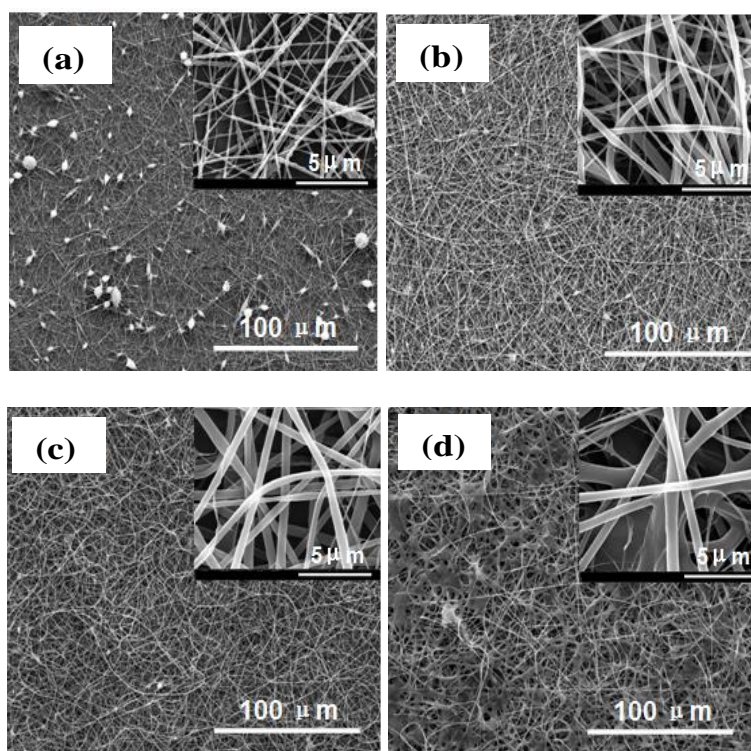


Figure 1. SEM images for electrospun PVDF fiber and the diameter distribution histograms with different contents (a) 12%, (b) 15%, (c) 17%, (d) 20%

Several Al sheets were cut into the same size as the electrode area and electrospun for 5 min to determine the thickness of the membranes. SEM side-view images are shown in Fig. 2. The thickness of the four membranes with different contents was about 12-15 μm .

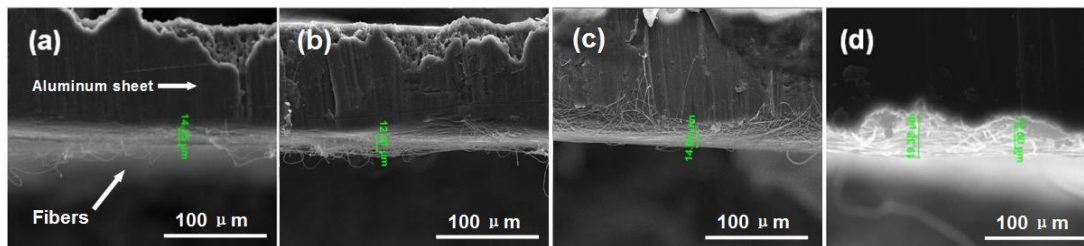
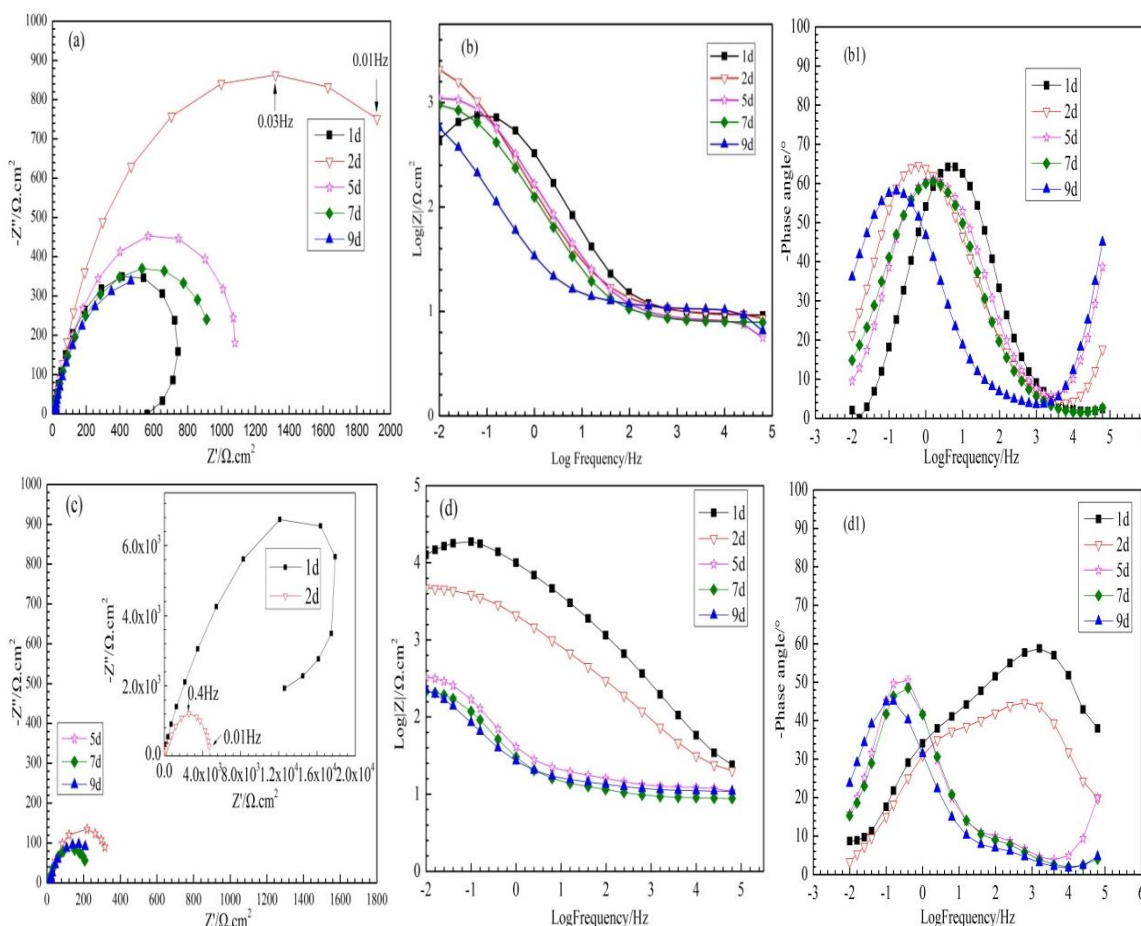


Figure 2. SEM images of (a) 12%, (b) 15%, (c) 17% and (d) 20% electrospun fiber membrane on aluminum sheet (Side View)

3.2. EIS measurements of electrodes coated with PVDF nanofiber membrane

The samples (bare electrode and electrodes coated with different contents of PVDF nanofiber membrane) were immersed in 3.5 wt. % solutions at different periods to investigate their electrochemical performance. The Nyquist and Bode plots are shown in Fig. 3.



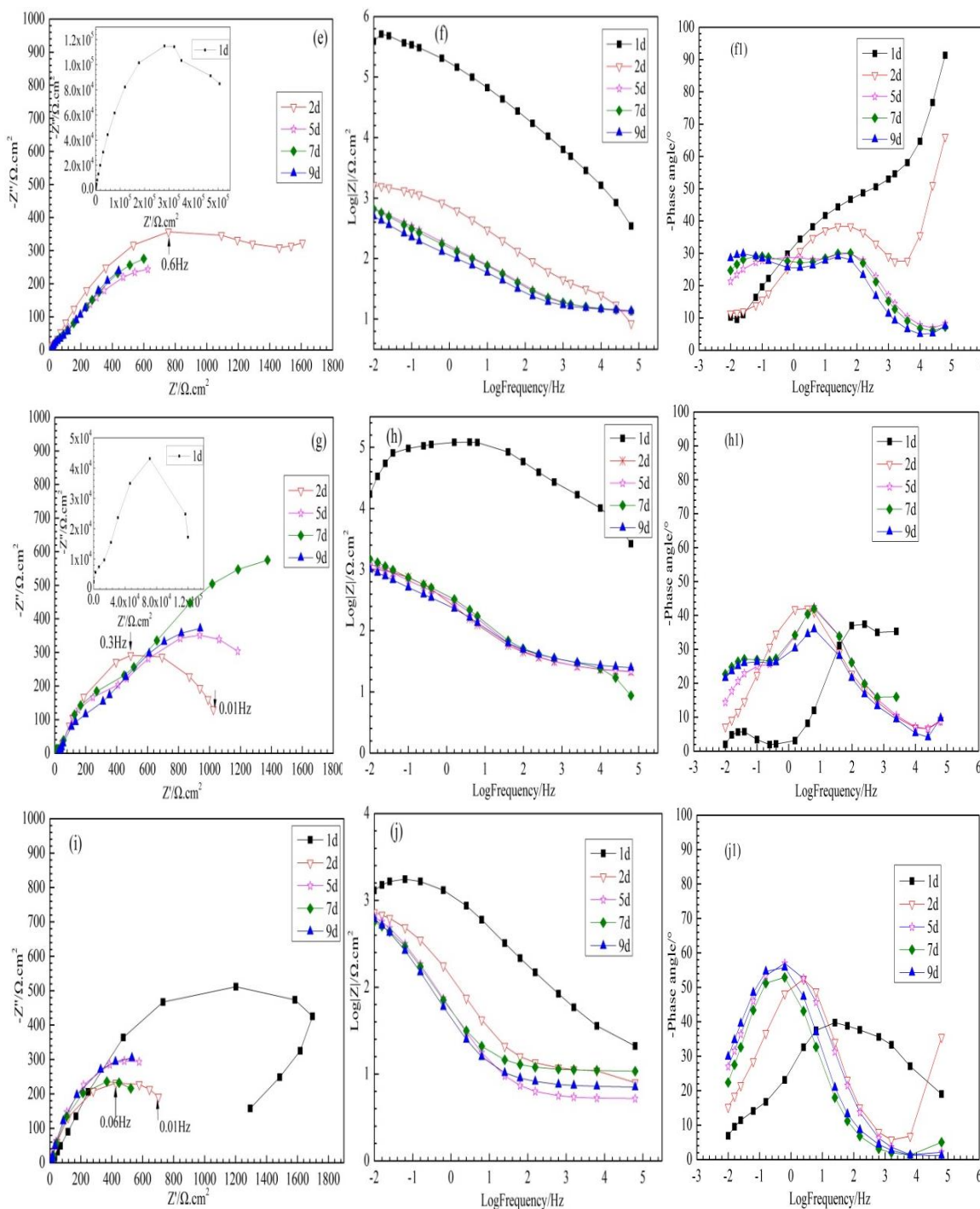


Figure 3. Nyquist and Bode plots of the samples immersed in 3.5 wt. % NaCl solution at different periods (a,b,b1) bare electrode, (c,d,d1) 12% PVDF, (e,f,f1) 15% PVDF, (g,h,h1) 17% PVDF and (i, j, j1) 20% PVDF

The Nyquist plots for bare electrode mainly displayed a capacitive loop at all immersion periods. The radius of the capacitive loop immersed for day 2 abruptly increased, then decreased and gradually fluctuated (Fig. 3a). In the Bode plots (Figs. 3b and 3b1), the low frequency impedance modulus fluctuated and there were two time constants during all the immersion time. The phase angles at low frequency decreased gradually. This result indicated that the metal surface was corroded on day

1, and the corrosion products accumulated on the surface and protected the metal for a short period, causing the radius of the capacitive loop increasing. However, the electrode was corroded further with immersion time.

Meanwhile, all the samples with PVDF nanofiber membranes exhibited a similar phenomenon, in which the radius of the capacitive loop on day 1 was considerably larger than that on the other days. Subsequently, the radius of the capacitive loop decreased abruptly (Figs. 3c, 3e, 3g and 3i).

For the 12% PVDF nanofiber membrane, the capacitive loop at day 1 was deformed (Fig. 3c), which was similar with EIS Nyquist plots of brass in relevant reference [7]. The reason was that time constant of absorption process was close to that of time constant of electrochemical reaction; two capacitive loops were overlapped, leading to a deformed capacitive loop. The radius of the capacitive loop was larger than that of the bare electrode for the day 2, meaning that the nanofiber membrane acted as a physical barrier to hinder entrance of the corrosive ions for a while. After that, the radius of the capacitive loop was gradually lower than that of the bare electrode. In the Bode plots, the low frequency impedance modulus was higher than that of bare electrode with about one order of magnitude for the first and second day, and then decreased rapidly (Fig.3d). The phase angles at low frequency were decreased and lower than that of bare electrode (Fig.3d1). Moreover, the time constants at low frequency were shifted to the lower frequency with immersion time. It was because that the nanofiber membrane acted as physical barrier layer and could protect the metal for two days. Due to existence of beaded structure for the nanofiber membrane, some porosity was formed, leading to entrance of the corrosive media and occurrence of local corrosion of the metal.

The Nyquist plots for the 15% and 17% nanofiber membranes exhibited a nearly similar tendency, but were different from those of the other membranes (Fig.3e, 3g). The radius of capacitive loop for the 15% and 17% nanofiber membranes at day 1 was higher than that of 12% with more than one order of magnitude, and the capacitive loops weren't deformed. Prolonging with immersion time, there were two obvious capacitive loops for the 15% and 17% nanofiber membranes. In the Bode plots, the low frequency impedance modulus for the 15% PVDF membrane on day 1 was about $10^6 \Omega \text{ cm}^2$. But it decreased quickly to be about $10^3 \Omega \text{ cm}^2$ with immersion time, which was still higher than that of 12% PVDF nanofiber membrane (Fig.3f). There were two time constants and shifted to the lower frequency with immersion time (Fig.3f1). However, the low frequency impedance modulus for the 17% PVDF membrane was more stable than that of 15% PVDF except on day 1 (Fig. 3h). It kept constant at about $10^3 \Omega \text{ cm}^2$. The lines at high frequency corresponding to the membrane capacitance were overlapped and didn't shift to the low frequency. The two time constants at high and low frequency didn't change much with immersion time (Fig. 3h1). It meant that capacitance and resistance of the nanofiber membrane corresponding to high frequency time constant were steady during immersion period. The results indicated that the 17% nanofiber membrane had better protection performance than that of 15% nanofiber because of its much more even fiber diameter and compact structure. However, both of the 15% and 17% nanofiber membranes played much better role of physical barrier than that of 12% membrane, and could impede entrance of corrosive media for some time.

As for the 20% PVDF nanofiber membranes, the shapes of Nyquist plots were similar to those of the bare electrode. The capacitive loop at day 1 was deformed, and the radius of capacitive loop at

day 1 was larger than that of the other days (Fig. 3i). In the Bode plots, the low frequency impedance modulus was about $10^3 \Omega \text{ cm}^2$, which was similar to that of bare electrode. The lines at high frequency shifted to the low frequency with immersion time, indicating that the nanofiber membrane capacitance changed gradually and didn't keep stable (Fig. 3j). The shape of phase angle-frequency curves was the same as that of bare electrode except for that on day 1 (Fig. 3j1). It demonstrated that the membrane played minor role to protect the metal because of its lamellar and loose structure. The electrolyte could easily penetrate into the surface of the substrate and caused it to be corroded.

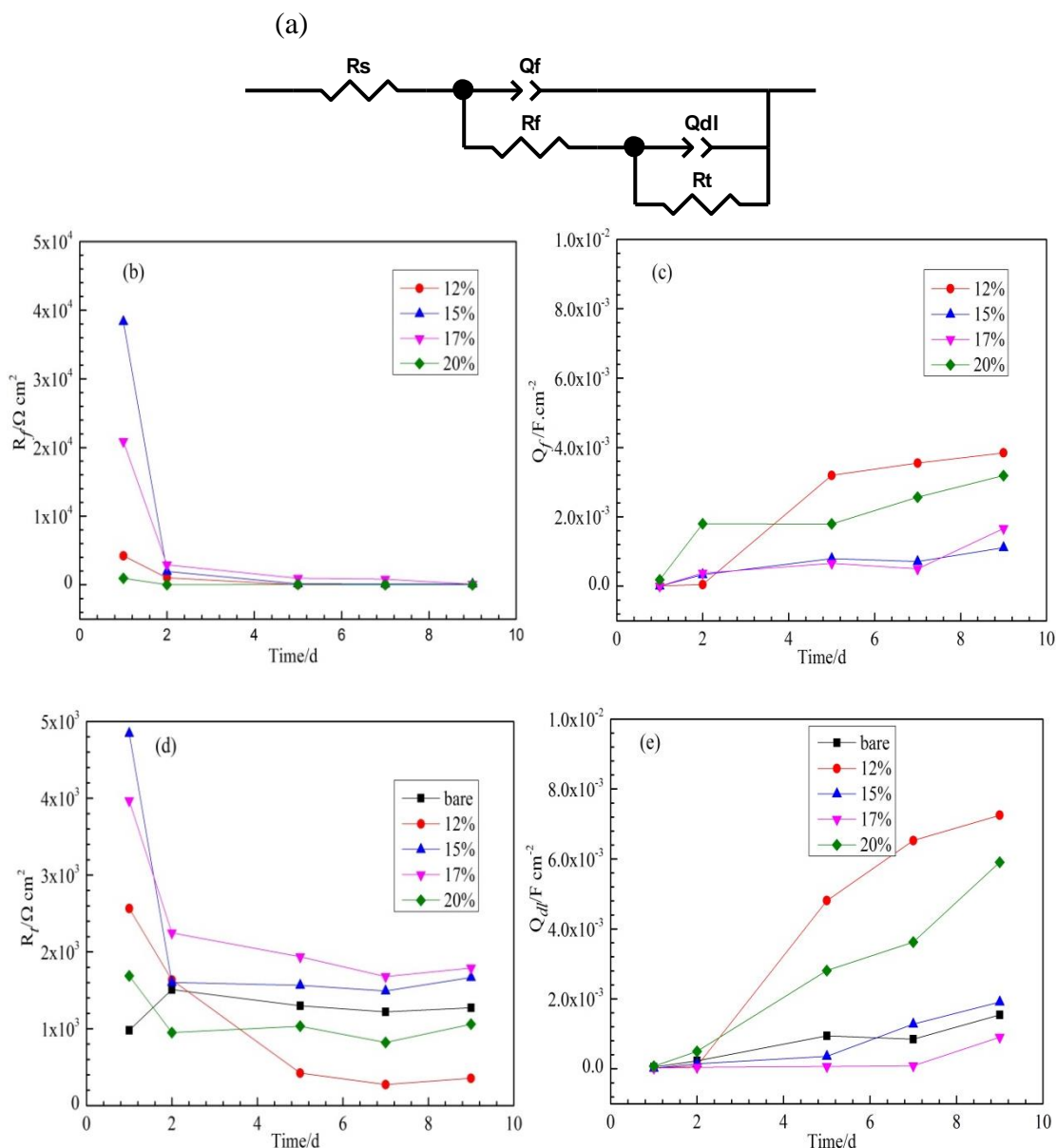


Figure 4. Representative equivalent circuit used for the EIS data and fitted parameters (a) equivalent circuit, (b) R_f , (c) Q_f , (d) R_t , (e) Q_{dl}

An equivalent electrical circuit is frequently used to analyze the impedance spectra of samples. A model of $R_s\{Q_f [R_f (Q_{dl}R_t)]\}$ was used to fit the EIS data as shown in Fig. 4a. In the equivalent

circuit, R_s is the solution resistance; Q_f and Q_{dl} are the constant phase elements that represent the capacitance of a nanofiber membrane and the double-charged layer, respectively; R_t is the charge-transfer resistance, which is used to simulate the electrochemical process at the metal interface (Faradic reaction) and R_f is the resistance of a nanofiber membrane [25].

The fitted parameters of the samples as a function of immersion time are shown in Fig.4b-4e. It could be found that for the 17% PVDF nanofiber membrane, its R_f and R_t was higher than those of the other nanofiber membrane (Figs. 4b and 4d) and decreased slowly with immersion time. Furthermore, its Q_f and Q_{dl} were least for all the nanofiber membrane and changed little with immersion time (Fig. 4c, 4e). For the other content of PVDF nanofiber membrane, the R_f and R_t decreased and the Q_f and Q_{dl} increased with immersion time, which was more obvious for the 12% PVDF membrane than the others. This phenomenon was attributed to absorbing of the water with high dielectric constant during immersion period, causing increasing of Q_f and decreasing of R_f , which in turn made decrease in R_t and increase in Q_{dl} . The fitted parameters meant that the 17% PVDF nanofiber membrane had the best protection performance among all the PVDF nanofiber membranes, because of its compactness and uniform thickness (Fig. 1c), which could effectively impede the entrance of corrosive ions and the metal substrate had the least corrosion rate. The 12% PVDF membrane had the worst protection performance due to existence of bead structure.

The above results indicated that the nanofiber membranes could protect the metal for some days [5-9, 11]. Moreover, the morphology of the nanofiber membrane had some effect on its protection performance. The more compact and uniform of the nanofiber, the better protection property it has. This result could also be verified by comparing electrospun nanofiber membrane with dip-coating membrane, and the nanofiber membrane had better anticorrosion protection than that of dip-coating membrane due to its extraordinary compact microstructure [8, 9].

3.3 Morphology of the substrates

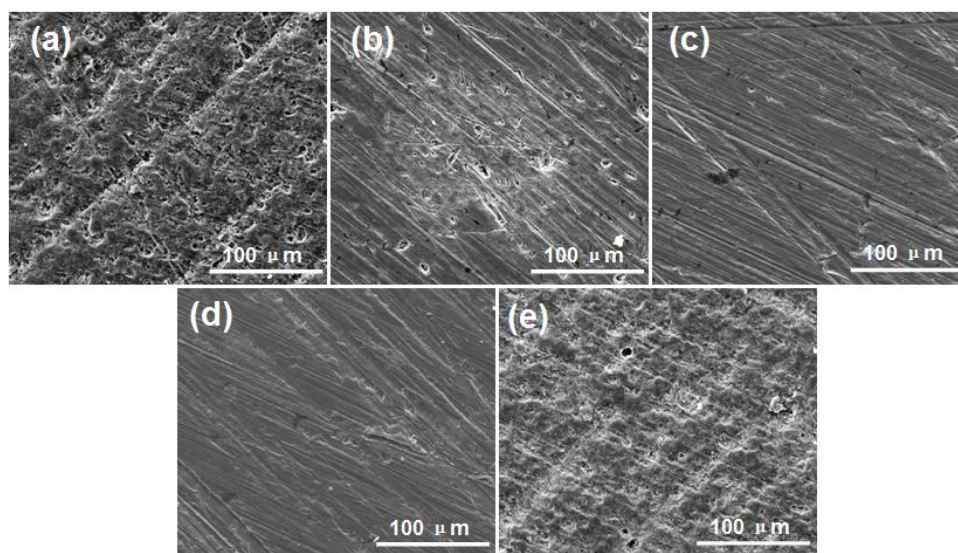


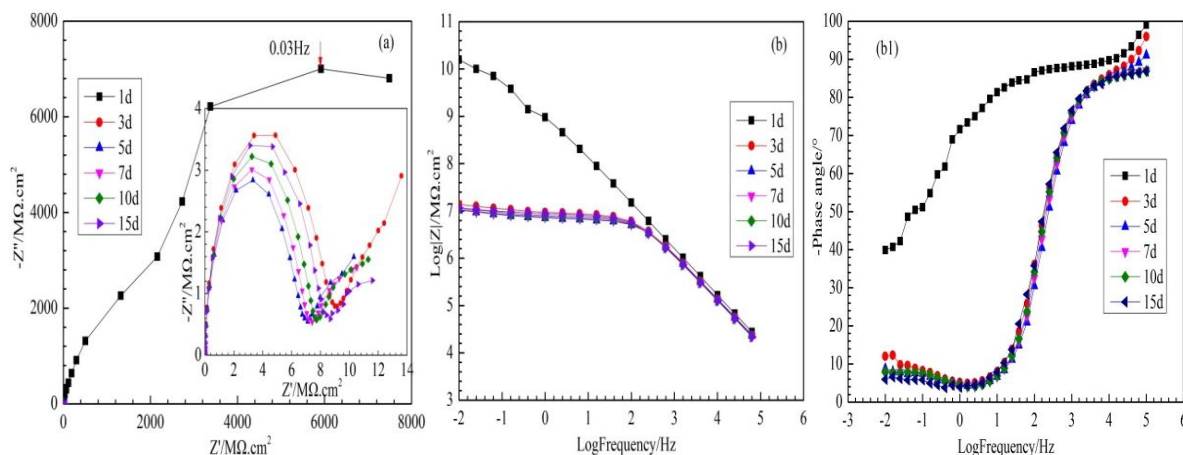
Figure 5. SEM images of the metal substrate after corrosion (a) bare electrode, (b) 12% PVDF, (c) 15% PVDF, (d) 17% PVDF, (e) 20% PVDF

After being immersed for 9 d, the samples were taken out of the electrolyte solution and cleaned with distilled water. The nanofiber membranes were subsequently removed using a soft paper. The morphologies of the metals are shown in Fig. 5.

The bare electrode was severely corroded (Fig. 5a) and exhibited general corrosion. The substrate protected by the 12% PVDF nanofiber membrane demonstrated pit corrosion (Fig.5b). However, for the 15% and the 17% PVDF nanofiber membranes, the substrates had similar morphologies, and no obvious corrosion was observed (Figs.5c and 5d). The substrate for the 20% PVDF nanofiber membrane showed a similar morphology to that of the bare electrode (Fig.5e), and exhibited general corrosion. The differences in substrate morphology further verified that the morphology of the nanofiber membrane significantly affected its protection property. The bead structure in the nanofiber caused some porosity, where the corrosive media could penetrate into the surface of the metal, leading to occurrence of pit corrosion. The compact and even thickness of nanofiber membrane protected the metal well.

3.4 EIS measurements of the PVDF/epoxy composite coating

The 17% PVDF/epoxy resin composite coating and pure epoxy resin coating were immersed in 3.5 wt. % solutions at different periods to investigate their electrochemical performance. The Nyquist and Bode plots are shown in Fig. 6. It can be found that for the pure epoxy resin coating, the coating had the characteristic of a perfect capacitor with high impedance modulus at the initial immersion stage (Fig.6a). With prolonged immersion time, the radius of capacitive loop decreased abruptly and the second capacitive loop appeared. The impedance modulus at low frequency decreased rapidly from 10^{10} to $10^7 \Omega \cdot \text{cm}^2$ after immersion for 3 days (Fig. 6b), and a horizontal line section appeared at middle frequency, meaning that the coating began to be delaminated. It indicated that the epoxy resin coating began to degrade and lost its protection performance [25]. The electrolyte solution penetrated through coating matrix and reached the metal surface to initiate the corrosion process. The second time constant appeared at low frequency after immersion for 3 days. But the phase angles at high frequency didn't change much with immersion time (Fig. 6b1).



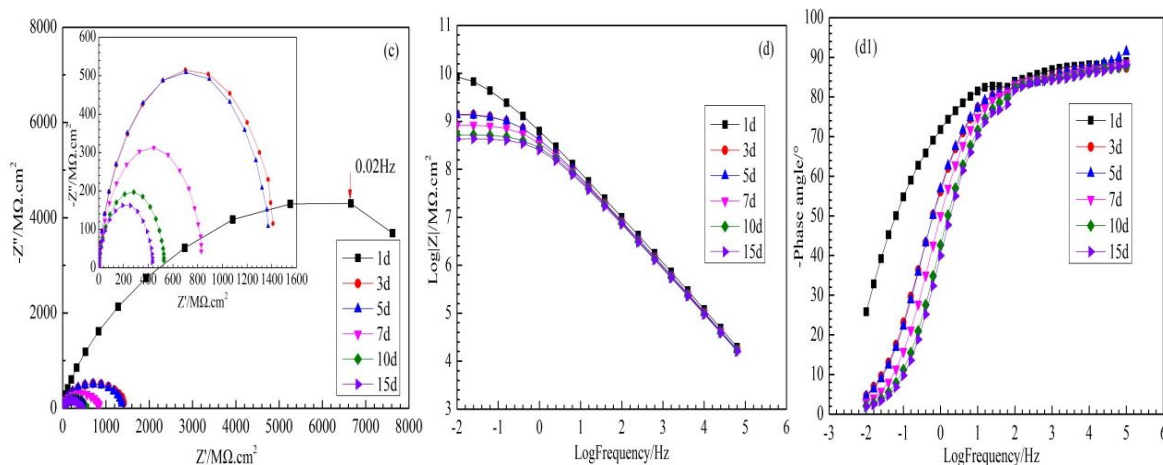


Figure 6. Nyquist and Bode plots of the coatings immersed in 3.5 wt. % NaCl solution at different periods (a, b, b1) pure epoxy resin coating, (c, d, d1) 17% PVDF /epoxy composite coating

For the composite coating, it also had the characteristic of a perfect capacitor at the initial immersion stage (Fig.6c). Then the radius of capacitive loops decreased gradually. However, the Nyquist plots mainly displayed one capacitive loop during all the immersion time. Meanwhile, the radius of capacitive loops was higher than that of pure epoxy resin with 2 orders of magnitude. In the Bode plots, the low frequency impedance modulus was more than $10^8 \Omega \cdot \text{cm}^2$ after 3 days immersion, and higher than that of pure epoxy resin coating with about 2 orders of magnitude (Fig. 6d). The lines at high frequency corresponding to the coating capacitance were overlapped and didn't shift to the low frequency with immersion time, meaning that the penetration of corrosive media was saturated and the capacitance of the composite coating wasn't increased further due to increasing of dielectric constant. There was only one time constant during immersion time (Fig. 6d1).

This phenomenon indicated that the composite coating had better protection property than that of pure epoxy resin coating. It was due to physical barrier of nanofiber membrane, as well as its pigment function in the composite coating. The longitudinal section of the coating is shown in Fig.7. It could be found that the nanofibers were distributed evenly in the coating, and the interface between nanofiber and epoxy resin was bonded together, which improved mechanical and protection property of the coating to some extent [26, 27]. The nanofiber blocked the pathways of the electrolyte in the coating and hindered the action of the electrolyte with the steel substrate. As a result, the enhanced pore resistance of the composite coating retarded further corrosion of the underlying steel substrate. Furthermore, the PVDF nanofiber had characterization of hydrophobicity, strong polarity, chemical corrosion resistance and excellent mechanical properties, enhancing hydrophobicity of the composite coating and improving its protection property, as well as its mechanical property. Based on the above information, it could be inferred that the PVDF nanofiber was a favorite and potential pigment to improve protection performance of the organic coatings.

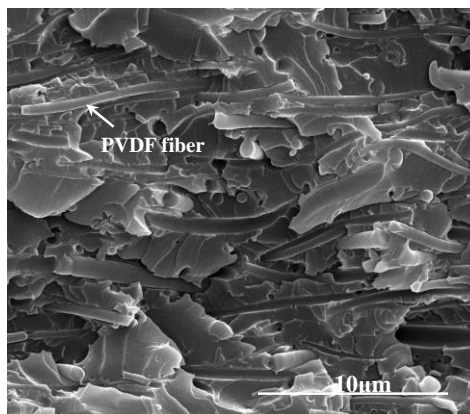


Figure 7. SEM image of longitudinal section of the composite coating

4. CONCLUSION

Different contents of PVDF solution was electrospun to prepare nanofiber membrane. It can be seen that the PVDF solution content had an important effect on the morphology of the nanofiber membranes. If the concentration of solution was low, some beads were observed in the nanofiber. The bead may disappear and the nanofiber became more and more uniform with increasing of content. However, when the content was too high, the electric field force couldn't make the droplets thoroughly split into thin thread. It caused a lamellar structure to be evident. 17% PVDF had the best nanofiber morphology with uniform thickness and compactness.

EIS results indicated that the morphology of the nanofiber membrane significantly influenced their protection performance. The more compact and uniform of the nanofiber, the better protection property it had. The nanofiber membranes can improve protection performance of the composite coating because of its barrier function, hydrophobicity, strong polarity and chemical corrosion resistance.

References

1. D. H. Reneker and I. Chun, *Nanotechnology*, 7 (1996) 216.
2. L.W. Ji, A. J. Medford and X. W. Zhang, *Polym. J.*, 50 (2009) 605.
3. W.E. Teo, R. Inai and S. Ramakrishna, *Sci. Technol. Adv. Mat.*, 12(2011) 43.
4. D. Lukáš, A. Sarkar, L. Martinová, K. Vodsed'álková and D. Lubasová, *Text. Prog.*, 41(2009) 59.
5. M. Sherif, M. Es-saheb, A. El-Zatahry, E. R. Kenawy and A. S. Alkaraki, *Int. J. Electrochem. Sci.*, 7 (2012) 6154.
6. A. Firouzi, C. D. Gaudio, F. R. Lamastra, G. Montesperelli and A. Bianco, *J. Appl. Polym. Sci.*, 132(2015) 41250.
7. M. Es-saheb, A. A. Elzatahry, M. Sherif, A. S. Alkaraki and E. R. Kenawy, *Int. J. Electrochem. Sci.*, 7 (2012) 5962.
8. A. Abdal-hay, N. A. M. Barakat and J. K. Lim, *Colloids Surf., A. Physicochem.*, 420 (2013) 37.
9. Y.Y. Zhao, Zh.M. Zhang and L.M. Yu, *React. Funct. Polym.*, 102 (2016) 20.

10. C. Menchaca, I. Castañeda, A. Soto-Quintero, R. Guardián and R. Cruz, *Int. J. Corros.*, 1(2012) 119.
11. J.W.Kim, H. M.Mousa, Ch. H.Park and Ch.S.Kim, *Appl. Surf. Sci.*, 396 (2017), 249.
12. B. Grignard, A. Vaillant, J. D. Coninck, M. Piens, A. M. Jonas and C. Detrembleur, *ACS. Langmuir*, 27(2011) 335.
13. X. F. Luo and P. T. Mather, *ACS Macro Lett.*, 2(2013) 152.
14. M. W. Lee, S. An, Ch.Lee, M. Liou, A. L. Yarin and S. S. Yoon, *J. Mater. Chem. A.*, 2(2014) 7045.
15. D. Han and A. Steckl, *ACS. Langmuir*, 25(2009) 9454.
16. J. H. Park and P. V. Braun, *Adv. Mater.*, 22(2010) 496.
17. A. Soto-Quintero, J. U. Chavarín, R. C. Silva, D. Bahena and C. Menchaca, *ECS Transactions*, 36(2011)119.
18. H. Fong, I. Chun and D.H. Reneker, *Polym. J.*, 40 (1999) 4585.
19. O. S. Yördem, M. Papila and Y. Z. Menciloğlu, *Mater. Des.*, 29 (2008) 34.
20. J. M. Deitzel, J. Kleinmeyer, D. Harris and N. C. Beck Tan, *Polym. J.*, 42 (2010) 261.
21. N. Choktaweasap, K. Arayanarakul, D. Aht-ong, C. Meechaisue and P. Supaphol, *Polym. J.*, 39(2007) 622.
22. E. S. Cozza, O. Monticelli, E. Marsano and P. Cebe, *Polym Int.*, 62(2013) 41.
23. M. Wang, D. Fang, N. Wang, S. Jiang, J. Nie, Q. Yu and G. Ma, *Polym. J.*, 55 (2014) 2188.
24. M. Dhanalakshmi, Ashish K. Lele and Jyoti P. Jog, *Mater. Today Communi.*, 3 (2015) 141.
25. Y.H. Dong, Q.Y. Zhang, X.M. Su and Q. Zhou, *Prog. Org. Coat.*, 76 (2013) 662.
26. M. M. Demir, N. Horzum, A. Taşdemirci and K. Turan, *ACS Appl. Mater. Interfaces*, 6 (2014) 21901.
27. M.W. Lee, S. An, H. S. Jo, S.S. Yoon and A. L. Yarin, *ACS Appl. Mater. Interfaces*, 7(2015)19546.

© 2017 The Authors. Published by ESG (www.electrochemsci.org). This article is an open access article distributed under the terms and conditions of the Creative Commons Attribution license (<http://creativecommons.org/licenses/by/4.0/>).